Seismic Inversion by Multi-dimensional Newtonian Machine Learning

Yuqing Chen[1], *Erdinc Saygin*[1] *1 and Gerard T. Schuster*[2]
[1]*Deep Earth Imaging Future Science Platform, CSIRO, Kensington, Australia*
[2] *King Abdullah University of Science and Technology (KAUST), Thuwal 23955-6900, Kingdom of Saudi Arabia.*

SUMMARY

Newtonian machine learning (NML) inversion has been shown to accurately recover the low-to-intermediate wavenumber information of subsurface velocity models. This method uses the wave-equation inversion kernel to invert the skeletonized data that is automatically learned by an autoencoder. The skeletonized data is a one-dimensional latent-space representation of the seismic trace. However, for a complicated dataset, the decoded waveform could lose some details if the latent space dimension is set to one, which leads to a low-resolution NML tomogram. To mitigate this problem, an autoencoder with a higher dimensional latent space is needed to encode and decode the seismic data. In this paper, we present a wave-equation inversion that inverts the multi-dimensional latent variables of an autoencoder for the subsurface velocity model. The multi-variable implicit function theorem is used to determine the perturbation of the multi-dimensional skeletonized data with respect to the velocity perturbations. In this case, each dimension of the latent variable is characterized one gradient and the velocity model is updated by the weighted sum of all these gradients. Numerical results suggest that the multi-dimensional NML inverted result can achieve a higher resolution in the tomogram compared to the conventional single-dimensional NML inversion.

INTRODUCTION

Full waveform inversion (FWI) has been shown to accurately invert seismic data for high-resolution velocity models (Lailly and Bednar, 1983; Tarantola, 1984; Virieux and Operto, 2009). However, FWI often suffers from the cycle-skipping problem which will trap the FWI in a local minimum (Bunks et al., 1995). One of the reasons cycle-skipping happens is that the data are very complex (i.e, wiggly in time), which means the FWI objective function is very complex and characterized by multiple minima. To mitigate the cycle-skipping problem, a series of skeletonized inversion methods have been proposed to reduce the nonlinearity of FWI by simplifying the complex waveform of seismic data (Lu et al., 2017). Luo and Schuster (1991a) uses the wave equation solution to invert the first arrival traveltimes for the background velocity model. Feng and Schuster (2019) uses the traveltime misfit function to invert for both velocity and anisotropic parameters in a vertical transverse isotropic medium. Instead of using traveltime as skeletonized data for inversion, Li et al. (2016) recovers the optimal S-velocity model by minimizing the difference between the observed and synthetic dispersion curve associated with surface waves. Dutta and Schuster (2016) finds the optimal subsurface Q_p model by using the peak/centroid-frequency shifts of the early arrivals.

The conventional skeletonized data, such as traveltime, often requires manual picking, which can be labor-intensive for large datasets. To solve this problem, Chen and Schuster (2019) proposed a Newtonian machine learning (NML) method suggesting that the skeletonized data can be automatically learned by an autoencoder network. For a well-trained autoencoder, the encoder and decoder network contains the common parts among all the training examples, however, the information preserved in the latent space, also denoted as the skeletonized representation, indicates their differences. Then the latent space skeletonized data can be inverted by the wave equation solution for the subsurface velocity model.

In the NML method, the seismic data is trained by an autoencoder with a one-dimensional latent space. For complicated data, the decoded waveform could lose some details which leads to a low-resolution inverted result. To mitigate this problem, in this paper, we present a multi-dimensional NML method that uses an autoencoder with a higher dimensional latent space to train the seismic data. Same as NML method, each training example is a one-dimensional seismic trace, but encoded into a higher dimensional latent space other than one. The misfit function measures the distances between the encoded observed and synthetic traces in a multi-dimensional space. And the multi-variable implicit function theorem is used to compute the perturbation of the skeletonized data with respect to the velocity. In this case, each latent space dimension has a gradient and the velocity model is updated by the weighted sum of all these gradients. This paper is organized into four sections. After the introduction, we show the theory of the multi-dimensional NML method. We next present a synthetic numerical result and conclude the paper in the last section.

THEORY

For the sake of briefness, we only introduce the theory of a two-dimensional NML method, where the higher-dimensional case can be derived in a similar way. A typical autoencoder with two-dimensional latent space is shown in Figure 1, which includes three parts: encoder, latent space, and decoder. The pink box in Figure 1 represents the encoder network that encodes the high-dimensional input seismic trace into a two-dimensional latent space using a series of neural layers with a decreasing number of neurons. The latent space indicated by the green box only has two neurons that preserve the effective low-dimension representations of the high-dimension input data. The decoder, which represented by the purple box, reconstructs the input data from the latent space using a series of neural networks with the increasing number of neurons.

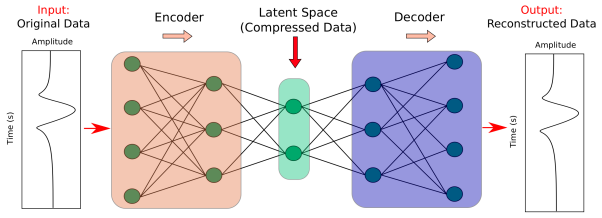

Figure 1: An example of an autoencoder architecture with two layers each for the encoder and decoder.

Theoretically, the capability of an autoencoder in reconstructing the input data is proportional to the number of neurons in the latent space. Figures 2a and 2g show two example of training data and their corresponding decoded waveforms are shown in Figures 2b and 2h, where the decoded waveforms are almost the same as the input data. These matches can be further proved by computing their waveform differences shown in Figure 2c and 2i, which are close to zero. However, for a complex waveform, such as the waveform shown in Figure 2d, the decoded result shown in Figure 3e can only recover part of the waveforms. The missing part can be seen in their data difference shown in Figure 2f. This waveform information missing is due to the number of neurons (one neuron) in the latent space is too small to fully capture all these waveform information.

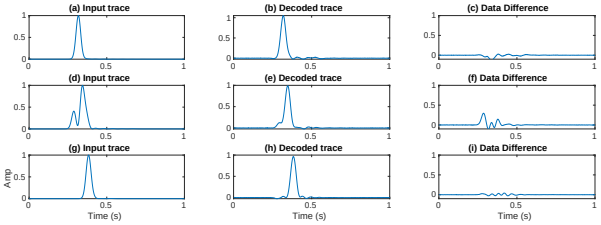

Figure 2: (a), (d) and (g) are three input training examples. (b), (e) and (h) are their corresponding decoded waveforms. (c), (f) and (i) are the waveform differences between the input and decoded waveforms.

The same data are encoded and decoded by an autoencoder with two-dimensional latent space. Compared to Figure 2e, the decoded waveform shown in Figure 3e has recovered all the complex waveform information of input data. And it's waveform difference shown in Figure 3f is close to zero now. Moreover, if you compare the waveform differences shown in Figures 3c, 3f and 3i with those waveform differences shown in Figure 2c, 2f and 2i, it clearly shows that the waveform differences become much smaller when we increase the number of latent space's neuron from one to two. Therefore, more waveform information can be preserved by these two latent space neurons.

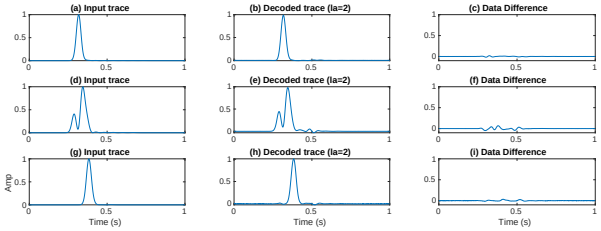

Figure 3: (a), (d) and (g) are three input training examples. (b), (e) and (h) are their corresponding decoded waveforms when the number of neurons in the latent space is equal to two. (c), (f) and (i) are the waveform differences between the input and decoded waveforms.

Theory of Two-dimensional NML

The misfit function of two-dimensional NML method can be written as

$$\varepsilon = \sum_s \sum_r \left[\Delta z_1(\mathbf{x}_r,\mathbf{x}_s)^2 + \Delta z_2(\mathbf{x}_r,\mathbf{x}_s)^2\right], \tag{1}$$

where $\mathbf{x}_r$ and $\mathbf{x}_s$ represent the location of receivers and sources. Δz_1 and Δz_2 indicate the encoded data difference in the first and second dimensions of the latent space, respectively. The gradient $\gamma(x)$ is given by

$$\begin{aligned}\gamma(\mathbf{x}) &= -\frac{\partial \varepsilon}{\partial v(\mathbf{x})} \qquad (2)\\ &= -\sum_s \sum_r \left[\left(\frac{\partial z_1(\mathbf{x}_r,\mathbf{x}_s)}{\partial v(\mathbf{x})}\right)^T \Delta z_1(\mathbf{x}_r,\mathbf{x}_s) + \left(\frac{\partial z_2(\mathbf{x}_r,\mathbf{x}_s)}{\partial v(\mathbf{x})}\right)^T \Delta z_2(\mathbf{x}_r,\mathbf{x}_s)\right].\end{aligned}$$

To compute the gradient γ, a connective function is required to connect the perturbation of the multi-dimensional latent variable δz_1 and δz_2 to the velocity perturbation δv. A cross-correlation function is defined as the connective function as

$$F(\tilde{z}_1,\tilde{z}_2;v) = \int p^{obs}_{(z_1-\tilde{z}_1,z_2-\tilde{z}_2)}(\mathbf{x}_r,t;\mathbf{x}_s)\, p^{syn}_{(z_1,z_2)}(\mathbf{x}_r,t;\mathbf{x}_s)dt \tag{3}$$

where $p^{syn}_{(z_1,z_2)}(\mathbf{x}_r,t;\mathbf{x}_s)$ represents a synthetic trace for a given background velocity model recorded at the receiver location x_r due to a source excited at location $\mathbf{x}_s$. The subscript z_1 and z_2 are the encoded value in the first and second dimension of the latent space, respectively. Similarly, $p^{obs}_{(z_1-\tilde{z}_1,z_2-\tilde{z}_2)}(\mathbf{x}_r,t;\mathbf{x}_s)$ denotes a observed trace with the first and second encoded vaule equals to $z_1-\tilde{z}_1$ and $z_2-\tilde{z}_2$ that has the same source and receiver location as $p^{syn}_{(z_1,z_2)}(\mathbf{x}_r,t;\mathbf{x}_s)$. Here, $\tilde{z}_1$ and $\tilde{z}_2$ represent the encoeded value shifts in the first and second latent space dimension, respectively. Using multi-variable implicit function theorem and equation 1 and **??**, we can get

$$\begin{aligned}\gamma(\mathbf{x}) &= \sum_s \sum_r \left\langle \begin{bmatrix} \frac{\partial \Delta z_1}{\partial v(\mathbf{x})} \\ \frac{\partial \Delta z_2}{\partial v(\mathbf{x})} \end{bmatrix}, \begin{bmatrix} \Delta z_1 \\ \Delta z_2 \end{bmatrix} \right\rangle \qquad (4)\\ &= \sum_s \sum_r \left\langle \begin{bmatrix} \frac{\partial^2 F}{\partial \tilde{z}_1^2} & \frac{\partial^2 F}{\partial \tilde{z}_1 \partial \tilde{z}_2} \\ \frac{\partial^2 F}{\partial \tilde{z}_1 \partial \tilde{z}_2} & \frac{\partial^2 F}{\partial \tilde{z}_2^2} \end{bmatrix}^{-1} \begin{bmatrix} \frac{\partial^2 F}{\partial \tilde{z}_1 \partial v} \\ \frac{\partial^2 F}{\partial \tilde{z}_2 \partial v} \end{bmatrix}, \begin{bmatrix} \Delta z_1 \\ \Delta z_2 \end{bmatrix} \right\rangle\end{aligned}$$

The velocity model is updated by the steepest gradient method

$$v(\mathbf{x})_{k+1} = v(\mathbf{x})_k + \alpha_k \gamma(\mathbf{x}) \tag{5}$$

where α_k is the step length and k indicates the iteration number.

NUMERICAL RESULTS

Data computed from a part of the SEAM model with a size of 157 x 135 grid points are used to test the multi-dimensional NML method. Figure 4a shows the true model and the finite-difference method is used to compute 52 acoustic shot gathers. These shots are evenly distributed along the source well located at x=10 m with a source interval of 30 m. Each shot contains 156 receivers that are evenly deployed at a spacing of 10 m along with the vertical receiver well, which is located 1340 m away from the source well. The source wavelet is a 12 Hz Ricker wavelet and a homogeneous velocity model that is shown in Figure 4b is used as the initial model.

Figures 2a and 2b show the tomograms that inverted by the one- and two-dimensional NML method, respectively. It can be seen that the two-dimensional NML result contains more details and has a higher resolution compared to the previous tomogram, which because the two-dimensional latent space has a stronger capability in preserving the complex waveform of the input data. Figure 6a shows the FWI inverted result based on the initial model, where the inverted result suffers severely from the cycle-skipping effects. However, the FWI inverted result shown in Figure 6b is very close to the true model, as the two-dimensional NML tomogram is used as the initial model in this case. Figures 7a and 7b show the velocity profile comparisons at x = 0.45 km and x = 0.85 km between the true model, initial model, one- and two-dimensional NML inverted tomogram, which represented by the blue solid, blue dashed, black and red lines, respectively. It clearly shows that the two-dimensional NML result (red line) can recover higher resolution details compared to the one-dimensional NML result (black line), especially at the area pointed by the green arrows.

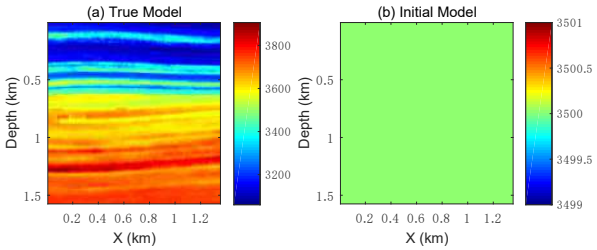

Figure 4: (a) True and (b) initial velocity models.

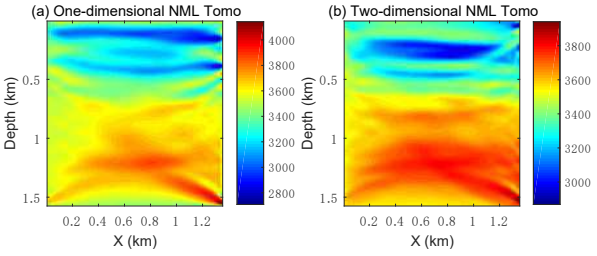

Figure 5: (a) one- and (b) two-dimensional NML inverted tomograms.

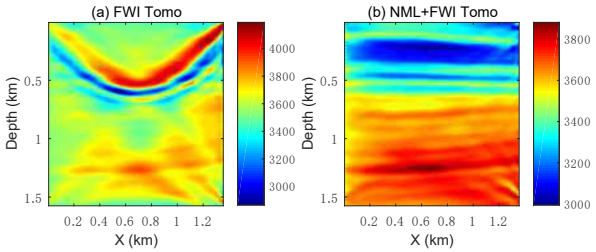

Figure 6: FWI inverted tomogram using the (a) initial model and (b) two-dimensional NML tomogram as the initial model.

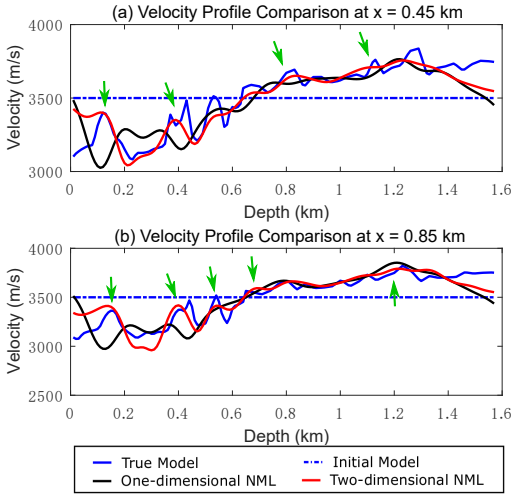

Figure 7: Velocity profile comparisons at (a) x = 0.45 km and (b) x = 0.85 km between the true model, initial model, one- and two-dimensional NML inverted tomogram, which represented by the blue solid, blue dashed, black and red lines, respectively.

CONCLUSIONS

We introduce a wave-equation method that finds the subsurface velocity model by minimizing the distance between the encoded observed and synthetic in a multi-dimensional latent space. Tests on synthetic data demonstrate the multi-dimensional NML method can recover the velocity model with higher resolution details when compared with the conventional one-dimensional NML method.

ACKNOWLEDGMENTS

We thanks to the Deep Earth Imaging Future Science Platform of CSIRO for funding and computing resources of CSIRO.

REFERENCES

Bunks, C., F. M. Saleck, S. Zaleski, and G. Chavent, 1995, Multiscale seismic waveform inversion: Geophysics, **60**, 1457–1473, doi: https://doi.org/10.1190/1.1443880.

Chen, Y., and G. T. Schuster, 2019, Seismic inversion by Newtonian machine learning: arXiv preprint arXiv:1904.10936.

Chen, S., L. Zimmerman, and J. Tugnait, 1990, Subsurface imaging using reversed vertical seismic profiling and crosshole tomographic methods: Geophysics, **55**, 1478–1487. doi: https://doi.org/10.1190/1.1442795.

Chen, Y., Z. Feng, L. Fu, A. AlTheyab, S. Feng, and G. Schuster, 2020, Multiscale reflection phase inversion with migration deconvolution: Geophysics, **85**, no. 1, R55–R73. doi: https://doi.org/10.1190/geo2018-0751.1.

Dutta, G., and G. T. Schuster, 2016, Wave-equation Q tomography: Geophysics, **81**, no. 6, R471–R484, doi: https://doi.org/10.1190/geo2016-0081.1.

Feng, S., and G. T. Schuster, 2019, Transmission+ reflection anisotropic wave-equation traveltime and waveform inversion: Geophysical Prospecting, **67**, 423–442, doi: https://doi.org/10.1111/1365-2478.12733.

Lailly, P., and J. Bednar, 1983, The seismic inverse problem as a sequence of before stack migrations: Conference on inverse scattering: Theory and application, 206–220.

Li, J., Z. Feng, and G. Schuster, 2016, Wave-equation dispersion inversion: Geophysical Journal International, **208**, 1567–1578, doi: https://doi.org/10.1093/gji/ggw465.

Lu, K., J. Li, B. Guo, L. Fu, and G. Schuster, 2017, Tutorial for wave-equation inversion of skeletonized data: Interpretation, **5**, no. 3, SO1–SO10, doi: https://doi.org/10.1190/INT-2016-0241.1.

Luo, Y., and G. T. Schuster, 1991a, Wave equation inversion of skeletalized geophysical data: Geophysical Journal International, **105**, 289–294, doi: https://doi.org/10.1111/j.1365-246X.1991.tb06713.x.

Luo, Y., and G. T. Schuster, 1991b, Wave-equation traveltime inversion: Geophysics, **56**, 645–653, doi: https://doi.org/10.1190/1.1443081.

Tarantola, A., 1984, Inversion of seismic reflection data in the acoustic approximation: Geophysics, **49**, 1259–1266, doi: https://doi.org/10.1190/1.1441754.

Virieux, J., and S. Operto, 2009, An overview of full-waveform inversion in exploration geophysics: Geophysics, **74**, no. 6, WCC1–WCC26, doi: https://doi.org/10.1190/1.3238367.